PERGAMON

International Journal of Solids and Structures 40 (2003) 3935–3954

INTERNATIONAL JOURNAL OF SOLIDS and STRUCTURES

www.elsevier.com/locate/ijsolstr

Scale-dependent plasticity potential of porous materials and void growth

Li Zhenhuan *, Huang Minsheng, Wang Cheng

Department of Mechanics, Huazhong University of Science and Technology, Wuhan 430074, P.R. China

Received 5 August 2002; received in revised form 15 March 2003

Abstract

In the present paper, a boundary value problem about the macroscopic response and its microscopic mechanism of a representative spherical cell with a spherical microvoid under axisymmetric triaxial tension has been theoretically investigated. To capture the size effects of local plastic deformation in the matrix, the strain gradient constitutive theory including the rotation and the stretch gradients developed by Fleck and Hutchinson [Strain gradient plasticity, in: J.W. Hutchinson, T.Y. Wu (Eds.), Advance in Applied Mechanics, vol. 33, Academic Press, New York, 1997, p. 295] is adopted. By means of the principle of minimum plasticity potential and the Lagrange multipliers method, the self-contained displacement field within the matrix has been computationally determined. Based on these, a size-dependent constitutive potential theory for porous material has been developed. The results indicate clearly that the microvoid evolution predicted by the present constitutive model displays very significant dependences on the void size especially when the radius a of microvoids is comparable with the intrinsic characteristic length l of the matrix. And when the void radius a is much lager than l, the present model can retrogress automatically to the Gurson model improved by Wang and Qin [Acta Mech. Solid. Sin. 10 (1989) 127, in Chinese].

Keywords: Strain gradient plasticity; Scale effect; Constitutive potential; Void growth; Damage theory

1. Introduction

The fracture in ductile materials generally results from the nucleation, growth and coalescence of microvoids. In the above-mentioned three sequential stages, the void growth takes the longest period of time and thus it is most important. Therefore, during the past thirty years, numerous theoretical models have been developed to describe the growth and coalescence of voids in the ductile materials. McClintock (1968) and Rice and Tracey (1969), respectively, investigated the growth of an isolated cylindrical void and a spherical void embedded in infinite media. Inspired by the work of R–T, Huang (1991) further carried out a more precise theoretical analysis on an infinite perfectly plastic solid containing a spherical void and found the R–T model underestimated the void growth rates about 50%. At their heels, Lee and Mear (1992)

* Corresponding author.
E-mail address: zhli68@public.wh.hb.cn (L. Zhenhuan).

0020-7683/03/$ - see front matter © 2003 Elsevier Science Ltd. All rights reserved.
doi:10.1016/S0020-7683(03)00178-1

further probed into the deformation of an incompressible power-law matrix containing a dispersion of aligned spheroidal voids. As everyone knows, the above-mentioned various damage models were derived from the infinite solids containing an isolated void as a result of ignoring the interaction of adjacent voids. For this reason, Gurson (1977) creatively presented the concept of a cell model, which possesses a finite volume and contains a spherical void, and theoretically developed a plastic potential function for a porous material. Although the original Gurson model has a few limitations (Pardoen and Hutchinson, 2000), it was the first to establish the internal relationship between the void evolution and plastic potential. In several subsequent works, various important extensions to the Gurson model have been suggested. To consider the influence of matrix strain hardening on the void evolution, Yamamoto (1978) roughly improved the Gurson model by amending the mean flow stress of the matrix material. Tvergaard (1981, 1982) introduced two adjustable parameters q_1 and q_2 to improve the original Gurson model. Following the same line as the Gurson model, Wang and Qin (1989) analyzed in detail void growth in a power-hardening matrix and obtained a macroscopic plastic potential for a porous material. Leblond et al. (1995) proposed a Gurson-type model incorporating an improved description of the strain hardening effect. In addition, Tvergaard and Needleman (1984) extended the Gurson model (GTN) to take account of the rapid loss of load carrying capacity during void coalescence. The improved GTN model and several of its extensions have been widely used to predict the ductile damage and fracture in metallic materials (Xia and Shih, 1995a,b, 1996; Ruggieri et al., 1996; Faleskog et al., 1998; Gao et al., 1998a,b). The beauty of these models is that they clearly reveal the key roles of the stress triaxiality and the effective plastic strain on void growth and coalescence. However, a number of researches have convincingly indicated that the crack propagation rate predicted by the classical damage models was rather sensitive to the finite element mesh adopted even if the FE mesh is sufficiently refined. To solve this problem, Bažant and Lin (1988) eloquently pointed out the importance of the nonlocal damage mechanism and suggested a kind of nonlocal damage theory. The basic idea of the nonlocal damage theory is that the evolution of the damage variable not only depends on the current value of the state variables at this point, but also has close dependence on its weighted average value in a zone surrounding this point. Based on this assumption, a scale parameter l_c characterizing the region size is introduced into the damage model. Several publications have demonstrated the ability of these nonlocal damage models to reduce the mesh sensitivity (Pijaudier-Cabot and Bažant, 1987; Sun and Hönig, 1994; Leblond et al., 1994; Tvergaard and Needleman, 1997), but the physical meaning of the scale parameter l_c is very unclear.

In recent years, the existence of a material length scale for plasticity is firmly supported by direct dislocation simulations (Cleveringa et al., 1997, 1998, 1999a,b; Bittencourt et al., 2003) and extensive laboratory experiments (Nix, 1989; De Guzman et al., 1993; Stelmashenko et al., 1993; Fleck et al., 1994; Lloyd, 1994; Ma and Clark, 1995; Poole et al., 1996; Nan and Clarke, 1996; Zhu et al., 1997, 1995; Mcelhaney et al., 1998; Nix and Gao, 1998; Stolken and Evans, 1998; Suresh et al., 1999; Gao and Huang, 2003). There is an intimate connection between size effects and gradients of plastic deformation, especially when the characteristic length scale of un-uniform plasticity deformation is the order of micron or submicron. The classic plastic constitutive relation cannot explain the size effects shown in experiments since they lack the characteristic length scale. Just in the last five years, various strain gradient plasticity theories including the length scale have been developed to describe the constitutive behavior of materials at the micron scale (Fleck and Hutchinson, 1993, 1994, 1997, 2001; Gao et al., 1999; Gao and Huang, 2001; Huang et al., 2000a,b; Acharya and Bassani, 2000; Acharya and Beaudoi, 2000). Although there exists rather notable differences in the physical and mechanical backgrounds of these theories, most of these models give satisfactory predictions in four kinds of typical microscale experiments such as the microtorsion (Fleck et al., 1994), the microbend (Stolken and Evans, 1998), the microindentation (Nix and Gao, 1998) and particle-reinforced metal-matrix composites (Lloyd, 1994). For porous materials, no direct experimental examinations have been carried out to validate the size effects on plastic deformation in the vicinity of the microvoids and the void growth, but there exists some indirect evidence indicating that smaller voids on the

micron scale are more difficult to grow in comparison to larger voids on the millimeter scale (Fleck and Hutchinson, 1997). As the first step to address the strain gradient theory for porous materials, Gologanu et al. (1995) generalized the Gurson model to consider the effects of the macroscopic strain gradient on the void evolution. However, since the matrix material is still modeled by the classic J_2 plastic constitutive relation, a persistent strain gradient effect results even when the void volume fraction is zero. Considering the inevitable existence of the residual deformation in the matrix, Li et al. (2002, 2003) investigated the growth and coalescence of voids in the matrix with a plastic gradient distribution. In order to bring the issue of local strain gradient effect on the growth of a void to a close, Fleck and Hutchinson (1993) studied the growth of a spherical void in an infinite medium using the couple-stress (CS) plasticity theory. However, the assumed dominant deformation field driving the void expansion is spherically symmetric, therefore, the displacement field in the vicinity of microvoid is irrotational inducing no any rotation gradient. As a result, no significant size effects on void growth are captured by the CS plasticity theory. For this reason, Fleck and Hutchinson (1997) developed the generalized strain gradient (SG) plasticity theory including all second-order gradients of displacement components and affirmed that the growth rate of a smaller void is much slower than that of a larger void. At their heels, based on the MSG theory (Gao et al., 1999) and TNT theory (Gao and Huang, 2001), Huang et al. (2000a) and Gao and Huang (2001), respectively, investigated the growth of a spherical void in an infinite medium subjected to remote spherically symmetric tension. Added to these, to consider the interaction of adjacent microvoids in the matrix material, Shu (1998) studied the deformation of a porous single crystal and its macroscopic stress carrying capacity based on the elasto-viscoplastic SG crystal plasticity formulation. However, the above-mentioned works are either limited to the cases in which only an isolated void in an infinite medium is considered or to the simple two-dimensional (2D) case. To our knowledge, it is difficult to find intensive investigations on the size effects of void evolution in porous materials subjected three-dimensional loadings in the existing literature.

Based on the above-mentioned background, we have been actively engaged in the development of a size-dependent plasticity potential for porous materials. In another paper (Huang et al., 2002), we have analyzed the response of a cell with a microvoid, following the same line of the Gurson model. But the displacement field assumed is very simple and is not self-contained. To overcome the above limitation, in the present paper, a displacement field with infinite terms satisfying the displacement compatibility equations is suggested. By the principle of minimum plasticity potential and the Lagrange multipliers method, the unknown coefficients in the series expansion of the displacement fields are numerically determined. Therefore, the present displacement field not only meets the displacement compatibility equation and the displacement boundary conditions, but also satisfies the equilibrium equations and thus is self-contained.

2. The plastic constitutive potential of porous materials

2.1. SG plasticity theory (Fleck and Hutchinson, 1997)

In the Cartesian reference coordinate system, the strain rate tensor $\dot{\varepsilon}_{ij}$ and the SG rate tensor $\dot{\eta}_{ijk}$ are related to the velocity components $\dot{u}_i$ by

$$\dot{\varepsilon}_{ij} = (\dot{u}_{i,j} + \dot{u}_{j,i})/2 \tag{1}$$

and

$$\dot{\eta}_{ijk} = \dot{u}_{k,ij} = \dot{\varepsilon}_{ik,j} + \dot{\varepsilon}_{jk,i} - \dot{\varepsilon}_{ij,k} \tag{2}$$

The SG rate tensor $\dot{\eta}_{ijk}$ can be decomposed into two parts as

$$\dot{\eta}_{ijk} = \dot{\eta}'_{ijk} + \dot{\eta}^{H}_{ijk} \tag{3}$$

where $\dot{\eta}'_{ijk}$ and $\dot{\eta}^{H}_{ijk}$ are, respectively, the deviatoric part and the hydrostatic part of $\dot{\eta}_{ijk}$.

For simplicity, elastic strain and plastic compressibility of the matrix are ignored. The condition of incompressibility can be stated as

$$\dot{\varepsilon}_{ii} = 0 \tag{4}$$

$$\dot{\eta}^{H}_{ijk} = (\delta_{ik}\dot{\eta}_{jpp} + \delta_{jk}\dot{\eta}_{ipp})/4 = 0 \tag{5}$$

Further, the deviatoric SG rate can be decomposed into three orthogonal parts as (Smyshlyaev and Fleck, 1996)

$$\dot{\eta}'_{ijk} = \dot{\eta}'^{(1)}_{ijk} + \dot{\eta}'^{(2)}_{ijk} + \dot{\eta}'^{(3)}_{ijk} \tag{6}$$

where

$$\dot{\eta}'^{(1)}_{ijk} = \dot{\eta}'^{S}_{ijk} - 1/5\left[\delta_{ij}\dot{\eta}'^{S}_{kpp} + \delta_{jk}\dot{\eta}'^{S}_{ipp} + \delta_{ki}\dot{\eta}'^{S}_{jpp}\right] \tag{7}$$

$$\dot{\eta}'^{(2)}_{ijk} = 1/6\lfloor e_{ikp}e_{jlm}\dot{\eta}'_{lpm} + e_{jkp}e_{ilm}\dot{\eta}'_{lpm} + 2\dot{\eta}'_{ijk} - \dot{\eta}'_{jki} - \dot{\eta}'_{kij}\rfloor \tag{8}$$

$$\dot{\eta}'^{(3)}_{ijk} = 1/6[-e_{ikp}e_{jlm}\dot{\eta}'_{lpm} - e_{jkp}e_{ilm}\dot{\eta}'_{lpm} + 2\dot{\eta}'_{ijk} - \dot{\eta}'_{jki} - \dot{\eta}'_{kij}] + 1/5[\delta_{ij}\dot{\eta}'^{S}_{kpp} + \delta_{jk}\dot{\eta}'^{S}_{ipp} + \delta_{ki}\dot{\eta}'^{S}_{jpp}] \tag{9}$$

In the above equations, e_{ijk} is the permutation tensor and $\dot{\eta}^{S}_{ijk}$ is the symmetric part of $\dot{\eta}_{ijk}$.

$$\dot{\eta}'^{S}_{ijk} = \lfloor\dot{\eta}'_{ijk} + \dot{\eta}'_{jki} + \dot{\eta}'_{kij}\rfloor/3 \tag{10}$$

In this work, the SG plasticity theory including the rotation and stretch gradients is adopted to describe the elastic–plastic stress vs. strain relation of the matrix. According to Fleck and Hutchinson's work (Fleck and Hutchinson, 1997), the multiaxial SG constitutive equation under proportionally and monotonically increasing deformation can be expressed as

$$\frac{\sigma_e}{\sigma_0} = \left(\frac{\dot{\xi}_e}{\dot{\xi}_0}\right)^n \tag{11}$$

where n and σ_0 are the strain hardening exponent and the reference stress, respectively, and $\dot{\xi}_0$ corresponds to $\dot{\xi}_e$ as $\sigma_e = \sigma_0$. The σ_e and $\dot{\xi}_e$ are the generalized effective stress and the generalized effective strain rate, which can be defined as

$$\sigma_e^2 = 3/2\sigma'_{ij}\sigma'_{ij} + l_1^{-2}\tau'^{(1)}_{ijk}\tau'^{(1)}_{ijk} + l_2^{-2}\tau'^{(2)}_{ijk}\tau'^{(2)}_{ijk} + l_3^{-2}\tau'^{(3)}_{ijk}\tau'^{(3)}_{ijk} \tag{12}$$

and

$$\dot{\xi}_e^2 = 2/3\dot{\varepsilon}'_{ij}\dot{\varepsilon}'_{ij} + l_1^2\dot{\eta}'^{(1)}_{ijk}\dot{\eta}'^{(1)}_{ijk} + l_2^2\dot{\eta}'^{(2)}_{ijk}\dot{\eta}'^{(2)}_{ijk} + l_3^2\dot{\eta}'^{(3)}_{ijk}\dot{\eta}'^{(3)}_{ijk} \tag{13}$$

where $\tau'^{(n)}_{ijk}$ is the deviatoric part of the high order stress tensor $\tau^{(n)}_{ijk}$; l_1, l_2 and l_3 are the intrinsic characteristic length of matrix, respectively.

Based on the above definition, for proportionally and monotonically loading, the size-dependent constitutive equations of the matrix under multiaxial stress and strain states can be further rewritten as

$$\sigma'_{ij} = \frac{2}{3}\frac{\sigma_e}{\dot{\xi}_e}\dot{\varepsilon}'_{ij} \tag{14}$$

$$\tau'^{(n)}_{ijk} = \frac{\sigma_e}{\dot{\xi}_e} l_n^2\dot{\eta}'^{(n)}_{ijk} \quad (n = 1, 2, 3, \text{the index } n\text{no sum}) \tag{15}$$

2.2. The macroscopic constitutive potential of porous materials

Introducing the high order stress tensor $\boldsymbol{\tau}$ and the SG rate tensor $\dot{\boldsymbol{\eta}}$, and noting that $\boldsymbol{\tau}$ is work rate conjugate to $\dot{\boldsymbol{\eta}}$, the microscope plastic potential ϕ of matrix can be expressed as

$$\begin{aligned}\varphi &= \int \sigma'_{ij}\,\mathrm{d}\dot{\varepsilon}'_{ij} + \int \tau'^{(1)}_{ijk}\,\mathrm{d}\dot{\eta}'^{(1)}_{ijk} + \int \tau'^{(2)}_{ijk}\,\mathrm{d}\dot{\eta}'^{(2)}_{ijk} + \int \tau'^{(3)}_{ijk}\,\mathrm{d}\dot{\eta}'^{(3)}_{ijk} \\ &= \frac{\sum_0}{2\dot{\xi}_0^n}\int \dot{\xi}_{\mathrm{e}}^{n-1}\,\mathrm{d}(\dot{\varepsilon}_{\mathrm{e}}^2 + l_1^2\dot{\eta}_{e1}^2 + l_2^2\dot{\eta}_{e2}^2 + l_3^2\dot{\eta}_{e3}^2) = \frac{\sigma_0}{(n+1)\dot{\xi}_0^n}\dot{\xi}_{\mathrm{e}}^{n+1}\end{aligned} \tag{16}$$

where $\dot{\varepsilon}_{\mathrm{e}} = \sqrt{\frac{3}{2}\dot{\varepsilon}_{ij}\dot{\varepsilon}_{ij}}$ and $\dot{\eta}_{em} = \sqrt{\dot{\eta}^{(m)}_{ijk}\dot{\eta}^{(m)}_{ijk}}$ $m = 1, 2, 3$.

Self-evidently, the above plastic potential ϕ can represent the constitutive behavior of the matrix. To describe the macroscopic responds of porous materials, we can consider a representative spheroidal cell with volume V_{cell} containing a spherical void. The macroscopic potential Φ of the porous material satisfying the inside and outside boundary conditions of the representative cell, the continuum condition, the plastic incompressibility of the matrix and the mechanical equilibrium equation can be stated as (Duva and Hutchinson, 1984)

$$\Phi = \frac{1}{V_{\mathrm{cell}}}\int_{V_{\mathrm{m}}} \phi\,\mathrm{d}V \tag{17}$$

where V_{m} is the volume of matrix in the cell.

Inserting (16) into (17) yields:

$$\Phi = \frac{1}{V_{\mathrm{cell}}}\frac{\dot{\xi}_0\sigma_0}{(n+1)}\int_{Vm}\left(\frac{\dot{\xi}_{\mathrm{e}}}{\dot{\xi}_0}\right)^{n+1}\mathrm{d}V \tag{18}$$

Duva and Hutchinson (1984) proposed that the macroscopic stresses can be related to the macroscopic potential Φ by

$$\sum\nolimits_{ij} = \frac{\partial\Phi}{\partial\dot{E}_{ij}} \tag{19}$$

3. The self-contained solution of a representative spherical cell with a spherical void

Many studies have already confirmed that the representative volume element (RVE) of the cell model can rationally describe the internal relations between the macroscopic mechanical responses and the microstructure of materials (Gurson, 1977; Koplik and Needleman, 1988; Wang and Qin, 1989). Fig. 1 shows the geometry of the spheroidal cell containing a spherical void, where a and b are the inside and outside radii of the cell, respectively. For convenience, the rectangular coordinates (x, y, z) and the spherical coordinates (r, θ, φ) are adopted.

3.1. The boundary value problem of the spheroidal cell

In the spherical coordinate system (r, θ, φ), the physical components of the strain rate tensor can be written as

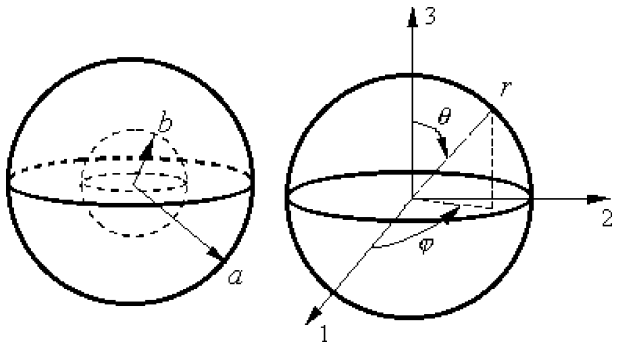

Fig. 1. Representative spherical cell with a spherical void: (a) representative cell model and (b) spherical coordinates frame.

$$\begin{cases} \dot{\varepsilon}_{rr} = \dfrac{\partial \dot{u}_r}{\partial r} \\ \dot{\varepsilon}_{\theta\theta} = \dfrac{1}{r}\dfrac{\partial \dot{u}_\theta}{\partial \theta} + \dfrac{\dot{u}_r}{r} \\ \dot{\varepsilon}_{\phi\phi} = \dfrac{1}{r\sin\theta}\dfrac{\partial \dot{u}_\phi}{\partial \phi} + \dfrac{\dot{u}_\theta}{r} ctg\theta + \dfrac{\dot{u}_r}{r} \\ \dot{\varepsilon}_{r\theta} = \dfrac{1}{2}\left(\dfrac{\partial \dot{u}_\theta}{\partial r} - \dfrac{\dot{u}_\theta}{r} + \dfrac{1}{r}\dfrac{\partial \dot{u}_r}{\partial \theta}\right) \end{cases} \tag{20}$$

In the rectangular coordinate system (x, y, z), the SG rate tensor $\dot{\eta}_{ijk}$ and rotation gradient rate tensor $\dot{\chi}_{ij}$ can be expressed as

$$\dot{\eta}_{ijk} = \dot{u}_{k,ij} \tag{21}$$

$$\dot{\chi}_{ij} = \frac{1}{2} e_{its} \dot{u}_{s,tj} = \frac{1}{2} e_{its} \dot{\eta}_{tjs} \tag{22}$$

So the physical components of the SG rate tensor and rotation gradient rate tensor in the spherical coordinate system (r, θ, φ) can be expressed respectively as

$$\dot{\eta}_{ijk} = \frac{\partial_j (A_k A_i T_{ki}) - A_k A_m T_{km} \Gamma^m_{ij} - A_m A_i T_{mi} \Gamma^m_{kj}}{A_i A_j A_k} \quad (i, j, k = r, \theta, \varphi) \tag{23}$$

and

$$\dot{\chi}_{ij} = \frac{\partial_j (A_i \theta_i) - A_m \theta_m \Gamma^m_{ij}}{A_i A_j} \quad (i, j, k, m = r, \theta, \varphi) \tag{24}$$

Here

$$T_{ij} = \frac{\partial_j \left(A_i \dot{u}_i\right) - A_m \dot{u}_m \Gamma^m_{ij}}{A_i A_j} \tag{25}$$

$$\theta_i = \frac{1}{2} e_{ijk} \frac{\partial_j \left(A_k \dot{u}_k\right)}{A_i} \tag{26}$$

where Γ_{ij}^{m} is the second Christoffel symbol and e_{ijk} is the permutation tensor. The non-zero components of Γ_{ij}^{m} in the spherical coordinate system (r,θ,φ) are:

$$\begin{cases} \Gamma_{\theta\theta}^{r} = -r, \quad \Gamma_{\varphi\varphi}^{r} = -r\sin^2\theta, \quad \Gamma_{\varphi\varphi}^{\theta} = -\sin\theta\cos\theta \\ \Gamma_{\theta r}^{\theta} = \Gamma_{r\theta}^{\theta} = \frac{1}{r}, \quad \Gamma_{\varphi r}^{\varphi} = \Gamma_{r\varphi}^{\varphi} = \frac{1}{r}, \quad \Gamma_{\varphi\theta}^{\varphi} = \Gamma_{\theta\varphi}^{\varphi} = \mathrm{ctg}\theta \end{cases} \tag{27}$$

For the spherical coordinates system (r,θ,φ), A_i can be expressed as

$$A_r = 1, \quad A_\theta = r, \quad A_\phi = r\sin\theta \tag{28}$$

To simplify the problem considered but not to lose generality, we assume that the outside boundary of the spherical cell is loaded by the axisymmetric macroscopic strain field as follows:

$$\begin{cases} \dot{E}_{11} = \dot{E}_{22},\ \dot{E}_{33} \neq 0 \\ \dot{E}_{ij} = 0,\ i \neq j \end{cases} \quad i,j = x,y,z \tag{29}$$

Thus

$$\dot{u}_\phi = 0, \quad \dot{\varepsilon}_{r\phi} = \dot{\varepsilon}_{\theta\phi} = 0 \tag{30}$$

In the spherical coordinate system, the matrix plastic incompressibility can be stated as:

$$\dot{\varepsilon}_{\theta\theta} + \dot{\varepsilon}_{\phi\phi} + \dot{\varepsilon}_{rr} = 0 \tag{31}$$

Inserting (20) into (31) obtains

$$\frac{\partial \dot{u}_r}{\partial r} + \left(\frac{\partial \dot{u}_\theta}{r\partial\theta} + \frac{\dot{u}_r}{r}\right) + \left(\frac{\dot{u}_\theta}{r}\mathrm{ctg}\theta + \frac{\dot{u}_r}{r}\right) = 0 \tag{32}$$

or

$$\frac{\partial}{\partial r}\left(r^2\dot{u}_r\sin\theta\right) + \frac{\partial}{\partial\theta}\left(r\dot{u}_\theta\sin\theta\right) = 0 \tag{33}$$

Apparently, to automatically satisfy (33), $\dot{u}_r$ and $\dot{u}_\theta$ can be formulated as

$$\begin{cases} \dot{u}_r = -\dfrac{1}{r^2\sin\theta}\dfrac{\partial\psi(r,\theta)}{\partial\theta} \\ \dot{u}_\theta = \dfrac{1}{r\sin\theta}\dfrac{\partial\psi(r,\theta)}{\partial r} \end{cases} \tag{34}$$

Without loss of generality, the function ψ can be assumed to be

$$\psi(r,\theta) = \overline{\psi}(r,\theta) + \tilde{\psi}(r,\theta) \tag{35}$$

where

$$\overline{\psi}(r,\theta) = A\cos\theta + B(r)\sin 2\theta \tag{36}$$

$$\tilde{\psi}(r,\theta) = \dot{\Xi}\sum_{m=1,3}^{\infty}\tilde{\psi}_m(r)\sin^2\theta\cos^m\theta \tag{37}$$

$$\tilde{\psi}_m(r) = a^3\sum_{k=0,1/3,2/3}^{\infty} a_{mk}\rho^k \tag{38}$$

$$\rho = (a/r)^3 \tag{39}$$

and $\dot{\Xi} = (2/3)(\dot{E}_{33} - \dot{E}_{11})$

Inserting (35)–(39) into (34) yields

$$\begin{cases} \dot{u}_r = \dot{\bar{u}}_r + \dot{\tilde{u}}_r \\ \dot{u}_\theta = \dot{\bar{u}}_\theta + \dot{\tilde{u}}_\theta \end{cases} \tag{40a}$$

where

$$\begin{cases} \dot{\bar{u}}_r = -\dfrac{1}{r^2 \sin\theta} \dfrac{\partial \overline{\psi}(r,\theta)}{\partial \theta} = \dfrac{A}{r^2} - \dfrac{B(r)}{r}(1 + 3\cos 2\theta) \\ \dot{\bar{u}}_\theta = \dfrac{1}{r \sin\theta} \dfrac{\partial \overline{\psi}(r,\theta)}{\partial r} = \dfrac{B'(r)}{r} \sin 2\theta \end{cases} \tag{40b}$$

$$\begin{cases} \dot{\tilde{u}}_r = -\dfrac{1}{r^2 \sin\theta} \dfrac{\partial \tilde{\psi}(r,\theta)}{\partial \theta} = -\displaystyle\sum_{m=1,3}^{\infty} \sum_{k=0,1/3}^{\infty} [a_{mk} \dot{\Xi} \rho^{1+k} r (\cos\theta)^{m-1} (2\cos^2\theta - m\sin^2\theta)] \\ \dot{\tilde{u}}_\theta = \dfrac{1}{r \sin\theta} \dfrac{\partial \tilde{\psi}(r,\theta)}{\partial r} = -\displaystyle\sum_{m=1,3}^{\infty} \sum_{k=0,1/3}^{\infty} a_{mk} \dot{\Xi} \rho^{1+k} k r \cos^m\theta \sin\theta \end{cases} \tag{40c}$$

Considering the microvoid concentration is very dilute, the macroscopic high order stress and the SG on the scale level of the representative cell are negligible. Therefore, the outside displacement boundary condition of cell can be expressed approximately as

$$\dot{U}_i \approx \dot{E}_{ij} X_j \text{ at } r = b \tag{41}$$

For the axisymmetric case, (41) can be rewritten further as

$$\begin{cases} \dot{U}_1 = \dot{E}_{11} X_1 = \dot{E}_{11} b \sin\theta \cos\phi \\ \dot{U}_2 = \dot{E}_{22} X_2 = \dot{E}_{11} b \sin\theta \cos\phi \\ \dot{U}_3 = \dot{E}_{33} X_3 = \dot{E}_{33} b \cos\theta \end{cases} \tag{42}$$

Transforming (42) to the spherical coordinates system (r, θ, φ) yields

$$\begin{cases} \dot{U}_r = b(\dot{E}_{11} \sin^2\theta + \dot{E}_{33} \cos\theta) = \dfrac{b(2\dot{E}_{11} + \dot{E}_{33})}{3} + \dfrac{b(\dot{E}_{33} - \dot{E}_{11})}{6}(1 + 3\cos 2\theta) \\ \dot{U}_\theta = b(\dot{E}_{11} - \dot{E}_{33}) \sin\theta \cos\theta = \dfrac{b}{2}(\dot{E}_{11} - \dot{E}_{33}) \sin 2\theta \\ \dot{U}_\phi = 0 \end{cases} \tag{43}$$

Comparing (43) with (40) one can obtain

$$\begin{cases} A = b^3 \dot{E}_m \\ B(b) = -b^3 \dot{E}_e / 6 \\ B'(b) = -b^2 \dot{E}_e / 2 \end{cases} \tag{44a}$$

and

$$\dot{\tilde{u}}_r(b) = 0, \ \dot{\tilde{u}}_\theta(b) = 0 \tag{44b}$$

or

$$\tilde{\psi}_m(b) = 0,\ \tilde{\psi}'_m(b) = 0 \tag{44c}$$

where $\dot{E}_m = \frac{1}{3}(2\dot{E}_{11} + \dot{E}_{33})$ and $\dot{E}_e = \dot{E}_{33} - \dot{E}_{11} = \frac{3}{2}\dot{\Xi}$.

According to (44a), the function $B(r)$ can be expressed as:

$$B(r) = -\frac{r^3}{6}(\dot{E}_{33} - \dot{E}_{11}) = -\frac{r^3}{6}\dot{E}_e \tag{45}$$

Substituting (44a) and (45) into (40b) yields

$$\begin{cases} \dot{\tilde{u}}_r = b^3\dot{E}_m/r + r\dot{E}_e(1 + 3\cos 2\theta)/6 \\ \dot{\tilde{u}}_\theta = -r\dot{E}_e \sin 2\theta/2 \end{cases} \tag{46}$$

Substituting (46) into (20) yields

$$\begin{cases} \dot{\tilde{\varepsilon}}_{rr} = -2b^3\dot{E}_m/r^3 + \dot{E}_e/6(1 + 3\cos 2\theta) \\ \dot{\tilde{\varepsilon}}_{\theta\theta} = b^3\dot{E}_m/r^3 + \dot{E}_e/6(1 - 3\cos 2\theta) \\ \dot{\tilde{\varepsilon}}_{\phi\phi} = b^3\dot{E}_m/r^3 - \dot{E}_e/3 \\ \dot{\tilde{\varepsilon}}_{r\theta} = -\sin 2\theta\dot{E}_e/2 \end{cases} \tag{47}$$

Substituting (40c) into (20) yields

$$\begin{cases} \dot{\tilde{\varepsilon}}_{rr} = \dot{\Xi}\sum\limits_{m=1,3}^{\infty}\sum\limits_{k=0,1/3}^{\infty} a_{mk}\rho^{k+1}t^{m-1}\alpha_{mk} \\ \dot{\tilde{\varepsilon}}_{\theta\theta} = \dot{\Xi}\sum\limits_{m=1,3}^{\infty}\sum\limits_{k=0,1/3}^{\infty} a_{mk}\rho^{k+1}t^{m-1}\beta_{mk} \\ \dot{\tilde{\varepsilon}}_{\phi\phi} = \dot{\Xi}\sum\limits_{m=1,3}^{\infty}\sum\limits_{k=0,1/3}^{\infty} a_{mk}\rho^{k+1}t^{m-1}\gamma_{mk} \\ \dot{\tilde{\varepsilon}}_{r\theta} = \frac{\dot{\Xi}}{2}\sum\limits_{m=1,3}^{\infty}\sum\limits_{k=0,1/3}^{\infty} a_{mk}\rho^{k+1}t^{m-2}\sin\theta\delta_{mk} \end{cases} \tag{48a}$$

where

$$\begin{cases} \alpha_{mk} = -(3k+2)[m - (2+m)t^2] \\ \beta_{mk} = (3k+1)m - [3k(m+1) + (2+m)]t^2 \\ \gamma_{mk} = m - (3k+m+2)t^2 \\ \delta_{mk} = -m(m-1) + [(m+1)(m+2) + 9k(k+1)]t^2 \\ t = \cos\theta \end{cases} \tag{48b}$$

Substituting (46) into (23) and (24) one obtains the non-zero components of the tensor $\dot{\bar{\eta}}_{ijk}$ and the tensor $\dot{\bar{\chi}}_{ij}$

$$\begin{cases} \dot{\bar{\eta}}_{rrr} = 6b^3\dot{\bar{E}}_m/r^4 \\ \dot{\bar{\eta}}_{\theta\theta r} = \dot{\bar{\eta}}_{r\theta\theta} = \dot{\bar{\eta}}_{\theta\theta r} = \dot{\bar{\eta}}_{r\phi\phi} = \dot{\bar{\eta}}_{\phi r\phi} = \dot{\bar{\eta}}_{\phi\phi r} = -3b^3\dot{\bar{E}}_m/r^4 \\ \dot{\bar{\chi}}_{ij} = 0 \end{cases} \tag{49a}$$

Substituting (40c) to (23) and (24), we can obtain

$$\begin{cases}
\dot{\tilde{\eta}}_{rrr} = \sum_{m=1,3}^{\infty}\sum_{k=0,1/3}^{\infty} \dot{\Xi} a_{mk}\rho^{1+k}t^{m-1}\Delta_{1mk}/r \\
\dot{\tilde{\eta}}_{rr\theta} = \sum_{m=1,3}^{\infty}\sum_{k=0,1/3}^{\infty} \dot{\Xi} a_{mk}\rho^{1+k}t^{m-2}\sin\theta\Delta_{2mk}/r \\
\dot{\tilde{\eta}}_{r\theta r} = \dot{\tilde{\eta}}_{\theta rr} = \sum_{m=1,3}^{\infty}\sum_{k=0,1/3}^{\infty} \dot{\Xi} a_{mk}\rho^{1+k}t^{m-2}\sin\theta\Delta_{3mk}/r \\
\dot{\tilde{\eta}}_{r\theta\theta} = \dot{\tilde{\eta}}_{\theta r\theta} = \sum_{m=1,3}^{\infty}\sum_{k=0,1/3}^{\infty} \dot{\Xi} a_{mk}\rho^{1+k}t^{m-1}\Delta_{4mk}/r \\
\dot{\tilde{\eta}}_{r\phi\phi} = \dot{\tilde{\eta}}_{\phi r\phi} = \sum_{m=1,3}^{\infty}\sum_{k=0,1/3}^{\infty} \dot{\Xi} a_{mk}\rho^{1+k}t^{m-1}\Delta_{5mk}/r \\
\dot{\tilde{\eta}}_{\theta\theta r} = \sum_{m=1,3}^{\infty}\sum_{k=0,1/3}^{\infty} \dot{\Xi} a_{mk}\rho^{1+k}t^{m-1}\Delta_{6mk}/r \\
\dot{\tilde{\eta}}_{\theta\theta\theta} = \sum_{m=1,3}^{\infty}\sum_{k=0,1/3}^{\infty} \dot{\Xi} a_{mk}\rho^{1+k}t^{m-2}\sin\theta\Delta_{7mk}/r \\
\dot{\tilde{\eta}}_{\theta\phi\phi} = \tilde{\eta}_{\phi\theta\phi} = \sum_{m=1,3}^{\infty}\sum_{k=0,1/3}^{\infty} \dot{\Xi} a_{mk}\rho^{1+k}t^{m-2}\sin\theta\Delta_{8mk}/r \\
\dot{\tilde{\eta}}_{\phi\phi r} = \sum_{m=1,3}^{\infty}\sum_{k=0,1/3}^{\infty} \dot{\Xi} a_{mk}\rho^{k+1}t^{m-1}\Delta_{9mk}/r \\
\dot{\tilde{\eta}}_{\phi\phi\theta} = \sum_{m=1,3}^{\infty}\sum_{k=0,1/3}^{\infty} \dot{\Xi} a_{mk}\rho^{1+k}t^{m-2}\sin\theta\Delta_{10mk}/r \\
\dot{\tilde{\chi}}_{r\phi} = \sum_{m=1,3}^{\infty}\sum_{k=0,1/3}^{\infty} \dot{\Xi} a_{mk}t^{m-2}\sin\theta\rho^{1+k}h_{1mk}/2r \\
\dot{\tilde{\chi}}_{\theta\phi} = \sum_{m=1,3}^{\infty}\sum_{k=0,1/3}^{\infty} \dot{\Xi} a_{mk}t^{m-1}\rho^{1+k}h_{1mk}/2r \\
\dot{\tilde{\chi}}_{\phi r} = \sum_{m=1,3}^{\infty}\sum_{k=0,1/3}^{\infty} \dot{\Xi} a_{mk}t^{m-2}\sin\theta\rho^{1+k}(3+3k)h_{1mk}/2r \\
\dot{\tilde{\chi}}_{\phi\theta} = \sum_{m=1,3}^{\infty}\sum_{k=0,1/3}^{\infty} \dot{\Xi} a_{mk}t^{m-1}\rho^{1+k}h_{2mk}/2r
\end{cases} \tag{49b}$$

Here

$$\Delta_{1mk} = 3(2+5k+3k^2)m - 3(2+5k+3k^2)(2+m)t^2$$

$$\Delta_{2mk} = -9k(2+5k+3k^2)t^2$$

$$\Delta_{3mk} = -3m(1+k)(1-m) - 3(1+k)(2+3k+3m+m^2)t^2$$

$$\Delta_{4mk} = -m(1+k)(9k+3) + 3(1+k)(2+3k+m+3km)t^2$$

$$\Delta_{5mk} = -3m(1+k) + 3(1+k)(2+3k+m)t^2$$

$$\Delta_{6mk} = (m^3+4m^2+8m+9km+12k+8)t^2 + (m^3-3m^2+2m)t^{-2} - (2m^3+m^2+9km+6)$$

$$\Delta_{7mk} = m(2+3k-2m-3km) + (4+12k+9k^2+6m+6km+2m^2+3km^2)t^2$$

$$\Delta_{8mk} = m(1-m) + (m^2 + 3m + 3km + 3k + 2)t^2$$

$$\Delta_{9mk} = -m(2 + 3k + m) + (4 + m)(2 + 3k + m)t^2$$

$$\Delta_{10mk} = 3k(2 + 3k + m)t^2$$

$$h_{1mk} = m(1-m) + (m^2 + 3m - 9k^2 - 3k + 2)t^2$$

$$h_{2mk} = (2m^3 + m^2 - 9k^2 - 3km + 3m) - (m^3 + 4m^2 - 9k^2m - 3km + 5m - 9k^2 - 3k + 2)t^2 - (m^3 - 3m^2 + 2m)/t^2$$

According to matrix plastic incompressibility, we obtain

$$\dot{\overline{\eta}}^H_{ijk} = \frac{1}{4}(\delta_{ik}\dot{\overline{\eta}}_{jpp} + \delta_{jk}\dot{\overline{\eta}}_{ipp}) = 0 \tag{50a}$$

$$\dot{\hat{\eta}}^H_{ijk} = \frac{1}{4}(\delta_{ik}\dot{\hat{\eta}}_{jpp} + \delta_{jk}\dot{\hat{\eta}}_{ipp}) = 0 \tag{50b}$$

Substituting (49) and (50) to (7)–(10) yields

$$\dot{\overline{\eta}}'_{ijk} = \dot{\overline{\eta}}'^{(1)}_{ijk} = \dot{\overline{\eta}}_{ijk}, \dot{\overline{\eta}}'^{(2)}_{ijk} = \dot{\overline{\eta}}'^{(3)}_{ijk} = 0 \quad i,j,k = r,\theta,\phi \tag{51a}$$

and

$$\begin{cases} \dot{\tilde{\eta}}'^{(1)}_{rrr} = \sum\limits_{m=1,3}^{\infty}\sum\limits_{k=0,1/3}^{\infty} \dot{\Xi} a_{mk} t^{m-3}\rho^{1+k} f_{1mk} \Big/ 15r \\ \dot{\tilde{\eta}}'^{(1)}_{r\theta\theta} = \dot{\tilde{\eta}}'^{(1)}_{\theta r\theta} = \dot{\tilde{\eta}}'^{(1)}_{\theta\theta r} = \sum\limits_{m=1,3}^{\infty}\sum\limits_{k=0,1/3}^{\infty} \dot{\Xi} a_{mk} t^{m-3}\rho^{1+k} f_{2mk} \Big/ 15r \\ \dot{\tilde{\eta}}'^{(1)}_{\phi r\phi} = \dot{\tilde{\eta}}'^{(1)}_{r\phi\phi} = \dot{\tilde{\eta}}'^{(1)}_{\phi\phi r} = \sum\limits_{m=1,3}^{\infty}\sum\limits_{k=0,1/3}^{\infty} \dot{\Xi} a_{mk} t^{m-3}\rho^{1+k} f_{3mk} \Big/ 15r \\ \dot{\tilde{\eta}}'^{(1)}_{\theta\theta\theta} = \sum\limits_{m=1,3}^{\infty}\sum\limits_{k=0,1/3}^{\infty} \dot{\Xi} a_{mk} t^{m-2}\sin\theta\rho^{1+k} g_{1mk} \Big/ 15r \\ \dot{\tilde{\eta}}'^{(1)}_{r\theta r} = \dot{\tilde{\eta}}'^{(1)}_{\theta rr} = \dot{\tilde{\eta}}'^{(1)}_{rr\theta} = \sum\limits_{m=1,3}^{\infty}\sum\limits_{k=0,1/3}^{\infty} \dot{\Xi} a_{mk} t^{m-2}\sin\theta\rho^{1+k} g_{2mk} \Big/ 15r \\ \dot{\tilde{\eta}}'^{(1)}_{\phi\theta\phi} = \dot{\tilde{\eta}}'^{(1)}_{\theta\phi\phi} = \dot{\tilde{\eta}}'^{(1)}_{\phi\phi\theta} = \sum\limits_{m=1,3}^{\infty}\sum\limits_{k=0,1/3}^{\infty} \dot{\Xi} a_{mk} t^{m-2}\sin\theta\rho^{1+k} g_{3mk} \Big/ 15r \end{cases} \tag{51b}$$

where

$$f_{1mk} = -3t^4(m^3 + 43m^2 + 72m^2k + 36m^2k^2 + 72k^2 + 144k + 64) + 3t^2\left[2m^3 + 2m^2 + 4m(8 + 18k + 9k^2)\right] - 3(m^3 - 3m^2 + 2m)$$

$$f_{2mk} = t^4\left[4m^3 + 15m^2 + (99k^2 + 168k + 62)m + 12(8 + 18k + 9k^2)\right] - t^2\left[8m^3 + 3m + (58 + 168k + 99k^2)m\right] + 4m^3 - 12m^2 + 8m$$

$$f_{3mk} = t^4\left[-m^3 + (52 - 48k - 9k^2)m + 12(8 + 18k + 9k^2)\right] - t^2\left[2m^3 - 3m^2 - (38 + 48k + 9k^2)m\right] + m^3 - 3m^2 + 2m$$

$$g_{1mk} = 3t^2\left[16 + 60k + 72k^2 + 27k^3 + 24m + 21km + 8m^2 + 12km^2\right] + 3\left[8m + 12km - 8m^2 - 12km^2\right]$$

$$g_{2mk} = -t^2\left[64 + 240k + 288k^2 + 108k^3 + 96m + 99km + 32m^2 + 33km^2\right] + \left[33km^2 + 32m^2 - 33km - 32m\right]$$

$$g_{3mk} = t^2\left[16 + 60k + 72k^2 + 27k^3 + 24m + 36km + 8m^2 - 3km^2\right] + \left[8m - 3km - 8m^2 + 3km^2\right]$$

Substituting (22) to (13), we obtain the generalized effective strain rate

$$\dot{\xi}_e^2 = \frac{2}{3}\dot{\varepsilon}'_{ij}\dot{\varepsilon}'_{ij} + l_1^2\dot{\eta}'^{(1)}_{ijk}\dot{\eta}'^{(1)}_{ijk} + \left(\frac{4}{3}l_2^2 + \frac{8}{5}l_3^2\right)\dot{\chi}'_{ij}\dot{\chi}'_{ij} + \left(\frac{4}{3}l_2^2 - \frac{8}{5}l_3^2\right)\dot{\chi}'_{ij}\dot{\chi}'_{ji} \tag{52}$$

By fitting the experimental data from ultra-thin beams in bending (Stolken and Evans, 1998), thin wires in torsion (Fleck et al., 1994), and microindentation (Stelmashenko et al., 1993; Ma and Clark, 1995; Nix, 1997), Begley and Hutchinson (1998) suggested

$$l_1 = \frac{1}{8}l, \quad l_2 = \frac{1}{2}l, \quad l_3 = \sqrt{\frac{5}{24}}l \tag{53}$$

where l is the characteristic length of matrix.

Substituting (53) into (52) yields

$$\dot{\xi}_e^2 = \frac{2}{3}\dot{\varepsilon}'_{ij}\dot{\varepsilon}'_{ij} + \frac{l^2}{64}\dot{\eta}'^{(1)}_{ijk}\dot{\eta}'^{(1)}_{ijk} + \frac{2l^2}{3}\dot{\chi}'_{ij}\dot{\chi}'_{ij} \tag{54}$$

According to (40a) and noting the plastic incompressibility, we can easily obtain

$$\dot{\varepsilon}'_{ij} = \dot{\varepsilon}_{ij} = \bar{\dot{\varepsilon}}_{ij} + \dot{\tilde{\varepsilon}}_{ij} \quad \dot{\eta}'^{(1)}_{ijk} = \bar{\dot{\eta}}'^{(1)}_{ijk} + \dot{\tilde{\eta}}'^{(1)}_{ijk} \quad \dot{\chi}'_{ij} = \dot{\chi}_{ij} = \bar{\dot{\chi}}_{ij} + \dot{\tilde{\chi}}_{ij} \tag{55}$$

Substituting (55) into (54) obtains

$$\dot{\xi}_e^2 = \frac{2}{3}(\bar{\dot{\varepsilon}}_{ij} + \dot{\tilde{\varepsilon}}_{ij})(\bar{\dot{\varepsilon}}_{ij} + \dot{\tilde{\varepsilon}}_{ij}) + \frac{l^2}{64}(\bar{\dot{\eta}}'^{(1)}_{ijk} + \dot{\tilde{\eta}}'^{(1)}_{ijk})(\bar{\dot{\eta}}'^{(1)}_{ijk} + \dot{\tilde{\eta}}'^{(1)}_{ijk}) + \frac{2l^2}{3}(\bar{\dot{\chi}}_{ij} + \dot{\tilde{\chi}}_{ij})(\bar{\dot{\chi}}_{ij} + \dot{\tilde{\chi}}_{ij}) = \bar{\dot{\xi}}_e^2(1 + \alpha^*) \tag{56}$$

where

$$\bar{\dot{\xi}}_e^2 = \frac{2}{3}\bar{\dot{\varepsilon}}_{ij}\bar{\dot{\varepsilon}}_{ij} + \frac{l^2}{64}\bar{\dot{\eta}}'^{(1)}_{ijk}\bar{\dot{\eta}}'^{(1)}_{ijk} + \frac{2l^2}{3}\bar{\dot{\chi}}_{ij}\bar{\dot{\chi}}_{ij},$$

$$\alpha^* = \frac{\dot{\tilde{\xi}}_e^2 + \frac{4}{3}\dot{\tilde{\varepsilon}}_{ij}\dot{\tilde{\varepsilon}}_{ij} + \frac{l^2}{32}\dot{\tilde{\eta}}'^{(1)}_{ijk}\dot{\tilde{\eta}}'^{(1)}_{ijk} + \frac{4l^2}{3}\dot{\tilde{\chi}}_{ij}\dot{\tilde{\chi}}_{ij}}{\bar{\dot{\xi}}_e^2}$$

and

$$\dot{\tilde{\xi}}_e^2 = \frac{2}{3}\dot{\tilde{\varepsilon}}_{ij}\dot{\tilde{\varepsilon}}_{ij} + \frac{l^2}{64}\dot{\tilde{\eta}}'^{(1)}_{ijk}\dot{\tilde{\eta}}'^{(1)}_{ijk} + \frac{2l^2}{3}\dot{\tilde{\chi}}_{ij}\dot{\tilde{\chi}}_{ij}$$

Substituting (56) into (18) and noting $V_{\text{cell}} = \frac{4}{3}\pi b^3$, we can easily obtain

$$\Phi = \frac{1}{V_{\text{cell}}}\int_{Vm}\varphi\,\mathrm{d}V = \frac{1}{V_{\text{cell}}}\frac{\dot{\xi}_0\sigma_0}{(n+1)}\int_{Vm}\left(\frac{\bar{\dot{\xi}}_e^2(1+\alpha^*)}{\dot{\xi}_0^2}\right)^{(n+1)/2}\mathrm{d}V$$

$$= \frac{3\sigma_0\dot{\xi}_0^{-n}}{2(n+1)b^3\pi}\int_0^{\pi}\sin\theta\,\mathrm{d}\theta\int_a^b\bar{\dot{\xi}}_e^{(n+1)}(1+\alpha^*)^{(n+1)/2}r^2\,\mathrm{d}r \tag{57}$$

If we assume $a^* \ll 1$, $(1+a^*)^{(n+1)/2}$ can be expanded by Taylor series and can be approximately expressed as

$$(1+a^*)^{(n+1)/2} \approx 1+\frac{n+1}{2}a^* \tag{58}$$

Substituting (58) into (57) yields

$$\Phi = \frac{3\sigma_0\dot{\xi}_0^{-n}}{2(n+1)b^3\pi}\int_0^{\pi}\sin\theta\,\mathrm{d}\theta\int_a^b \dot{\bar{\xi}}_{\mathrm{e}}^{(n+1)}r^2\,\mathrm{d}r + \frac{3\sigma_0\dot{\xi}^{-n}}{4b^3\pi}\int_0^{\pi}\sin\theta\,\mathrm{d}\theta\int_a^b \dot{\bar{\xi}}_{\mathrm{e}}^{(n+1)}\alpha^* r^2\,\mathrm{d}r \tag{59}$$

For convenience, we introduce the following dimensionless factors

$$\omega = \frac{2A}{\dot{\Xi}b^3} = \frac{3\dot{E}_m}{\dot{E}_{\mathrm{e}}} \quad x = \frac{2A}{\dot{\Xi}r^3} = \omega\left(\frac{b}{r}\right)^3 \quad \omega^* = \frac{\omega}{f} \quad f = \left(\frac{a}{b}\right)^3 \quad \lambda = \frac{l}{a} \tag{60}$$

where f is the void volume fraction, λ is the dimensionless length scale of the porous material relating to the characteristic length l of matrix material and the radius a of microvoids.

According to (47)–(49) and (51), we can obtain

$$\dot{\bar{\varepsilon}}_{\mathrm{e}}^2 = \frac{2}{3}\dot{\bar{\varepsilon}}_{ij}\dot{\bar{\varepsilon}}_{ij} = \frac{4A^2}{r^6} - \frac{A}{r^3}\dot{\Xi}h(t) + \dot{\Xi}^2 \tag{61a}$$

$$\dot{\bar{\varepsilon}}_{\mathrm{e}}^2 = \frac{2}{3}\dot{\bar{\varepsilon}}_{ij}\dot{\bar{\varepsilon}}_{ij} = \dot{\Xi}^2\sum_{m=1,3}^{\infty}\sum_{k=0,1/3}^{\infty}\sum_{n=1,3}^{\infty}\sum_{l=0,1/3}^{\infty}\lambda_{1mknl}t^{m+n-4}\rho^{k+l+2}a_{mk}a_{nl} \tag{61b}$$

$$\dot{\bar{\eta}}_{ijk}^{\prime(1)}\dot{\bar{\eta}}_{ijk}^{\prime(1)} = \frac{90b^6\dot{E}_m^2}{r^8} \tag{61c}$$

$$\dot{\bar{\eta}}_{ijk}^{\prime(1)}\dot{\bar{\eta}}_{ijk}^{\prime(1)} = \dot{\Xi}^2\sum_{m=1,3}^{\infty}\sum_{k=0,1/3}^{\infty}\sum_{n=1,3}^{\infty}\sum_{l=0,1/3}^{\infty}\lambda_{2mknl}t^{m+n-4}\rho^{k+l+2}a_{mk}a_{nl} \tag{61d}$$

$$\dot{\bar{\chi}}_{ij}\dot{\bar{\chi}}_{ij} = 0 \tag{61e}$$

$$\dot{\bar{\chi}}_{ij}\dot{\bar{\chi}}_{ij} = \dot{\Xi}^2\sum_{m=1,3}^{\infty}\sum_{k=0,1/3}^{\infty}\sum_{n=1.3}^{\infty}\sum_{k=0,1/3}^{\infty}\lambda_{3mnkl}t^{m+n-4}\rho^{k+l+2}a_{mk}a_{nl} \tag{61f}$$

$$\dot{\bar{\varepsilon}}_{ij}\dot{\bar{\varepsilon}}_{ij} = \dot{\Xi}^2\sum_{m=1,3}^{\infty}\sum_{k=0,1/3}^{\infty}J_{1mk}t^{m-1}\rho^{k+1}a_{mk} \tag{61g}$$

$$\dot{\bar{\eta}}_{ijk}^{(1)}\dot{\bar{\eta}}_{ijk}^{\prime(1)} = \dot{\Xi}^2\sum_{m=1,3}^{\infty}\sum_{k=0,1/3}^{\infty}J_{2mk}t^{m-1}\rho^{k+1}a_{mk} \tag{61h}$$

$$\dot{\bar{\chi}}_{ij}\dot{\bar{\chi}}_{ij} = 0 \tag{61i}$$

where

$$\begin{cases} t=\cos\theta \\ h(t)=6t^2-2 \\ \lambda_{1mnkl}=\dfrac{2}{3}\left[(\alpha_{mk}\alpha_{nl}+\beta_{mk}\beta_{nl}+\gamma_{mk}\gamma_{nl})t^2-(1-t^2)\delta_{mk}\delta_{nl}/2\right] \\ \lambda_{2mknl}=\dfrac{1}{64\times 15^2}\lambda^2\left(\dfrac{x}{\omega^*}\right)^{2/3}\left[\dfrac{1}{t^2}(f_{1mk}f_{1nl}+3f_{2mk}f_{2nl}+3f_{3mk}f_{3nl})\right. \\ \qquad\left.+(1-t^2)(g_{1mk}g_{1nl}+3g_{2mk}g_{2nl}+3g_{3mk}g_{3nl})\right] \\ \lambda_{3mknl}=\dfrac{1}{6}\lambda^2\left(\dfrac{x}{\omega^*}\right)^{2/3}\left\{\left[1+9(1+k)^2-9(1+k)^2t^2\right]h_{1mk}h_{1nl}+t^{-2}h_{2mk}h_{2nl}\right\} \\ J_{1mk}=-2\alpha_{mk}x+2[(\beta_{mk}-\delta_{mk})+(\alpha_{mk}-\beta_{mk}+\delta_{mk})t^2] \\ J_{2mk}=\dfrac{1}{160}\lambda^2\left(\dfrac{x}{\omega^*}\right)^{2/3}\left(\dfrac{3}{2}f_{3mk}-\dfrac{3}{2}f_{2mk}-f_{1mk}\right)x\Big/t^2 \end{cases}$$

Substituting (56), (60) and (61) into (59) leads to

$$\Phi=\overline{\Phi}+\tilde{\Phi} \tag{62a}$$

and

$$\bar{\Phi}=\frac{\sigma_0\dot{\xi}_0}{(n+1)}\left(\frac{\dot{\Xi}}{\dot{\xi}_0}\right)^{n+1}\bar{U}^*,\ \tilde{\Phi}=\frac{\sigma_0\dot{\xi}_0}{(n+1)}\left(\frac{\dot{\Xi}}{\dot{\xi}_0}\right)^{n+1}\tilde{U}^* \tag{62b}$$

where

$$\bar{U}^*=\frac{\omega}{2}\int_{-1}^{1}\mathrm{d}t\int_{\omega}^{\omega*}\frac{\Lambda^{n+1}}{x^2}\,\mathrm{d}x,$$

$$\tilde{U}^*=\frac{(n+1)\omega}{4}\left(\sum_{m=1,3}^{\infty}\sum_{k=0,1/3}^{\infty}\sum_{n=1,3}^{\infty}\sum_{l=0,1/3}^{\infty}A_{mkal}a_{mk}a_{nl}+\sum_{m=1,3}^{\infty}\sum_{k=0,1/3}^{\infty}B_{mk}a_{mk}\right),$$

$$A_{mknl}=\int_{-1}^{1}\mathrm{d}t\int_{\omega}^{\omega^*}\frac{\Lambda^{n-1}(\lambda_{1mknl}+\lambda_{2mknl}+\lambda_{3mknl})t^{m+n-4}\rho^{k+l+2}}{x^2}\,\mathrm{d}x,$$

$$B_{mknl}=\int_{-1}^{1}\mathrm{d}t\int_{\omega}^{\omega^*}\frac{\Lambda^{n-1}(J_{1mk}+J_{2mk})t^{m-1}\rho^{k+1}}{x^2}\,\mathrm{d}x,$$

$$\Lambda=\frac{\overline{\dot{\xi}_e}}{\dot{\Xi}}=\left[x^2-\frac{x}{2}h(t)+1+\frac{45}{128}\lambda^2\left(\frac{x^4}{\omega^*}\right)^{2/3}\right]^{1/2}$$

It is worth noting that the assumed displacement fields (40) only meet the displacement compatibility condition. For the actual displacement field, it must additionally meet the mechanical equilibrium condition and the displacement boundary conditions (44b) or (44c). This can be achieved by minimizing the plastic potential Φ with the boundary constraint conditions (44c). To this end, the Lagrange multiplier method is adopted to determine the undetermined coefficients a_{mk}.

According to (60), the boundary conditions (44c) can be rewritten as follows:

$$\sum_{k=0,1/3,2/3}^{\infty} a_{mk} f^{k+1} = 0 \qquad \sum_{k=0,1/3,2/3}^{\infty} k a_{mk} f^{k+1} = 0, \quad m = 1,3,5,\ldots \tag{63}$$

To make the plastic potential Φ minimum under the constraint conditions (63), the following governing equations must be satisfied:

$$\partial\left(\Phi + \sum_{m=1,3}^{\infty} \tau_m \sum_{k=0,1/3}^{\infty} a_{mk} f^{k+1} + \sum_{m=1,3}^{\infty} \omega_m \sum_{k=0,1/3}^{\infty} k a_{mk} f^{k+1}\right) \Big/ \partial a_{mk} = 0 \tag{64}$$

where τ_m and ω_m are the Lagrange multipliers, respectively.

Apparently, the relations (63) and (64) are a system of linear algebraic equations in the unknown coefficients a_{mk}. Once the coefficients a_{mk} are determined by numerical calculation, an approximate solution of the actual displacement field can be obtained. To obtain the coefficients a_{mk}, the double series of the trial field (40c) are truncated and the terms remaining in the approximate displacement fields correspond to $k = 0, 1/3, \ldots, (K-1)/3$ and $m = 1, 3, \ldots, (2M-1)$. As a part of the routine to calculate the coefficients a_{mk}, it is essential to perform accurate integrations of Φ over the volume V_{m} for the success of the above method. To do so, the integral domain is divided into 200×200 subdomains and in each subdomain the third-order Gaussian integrations have been performed.

3.2. The constitutive potential of porous materials

Similar with the Gurson model, the constitutive potential of the porous material can be expressed as a function of the macroscopic mean stress Σ_{m} and effective stress Σ_{e}. For this purpose, we substitute (62) into (19) and can obtain

$$\begin{cases} \Sigma_{\mathrm{m}} = \dfrac{\Sigma_{11} + \Sigma_{22} + \Sigma_{33}}{3} = \dfrac{1}{3}\left(2\dfrac{\partial \Phi}{\partial \dot{E}_{11}} + \dfrac{\partial \Phi}{\partial \dot{E}_{33}}\right) = \dfrac{2}{3}\dfrac{\sigma_0}{(1+n)}\left(\dfrac{\dot{\Xi}}{\dot{\xi}_0}\right)^n \dfrac{\partial(\bar{U}^* + \tilde{U}^*)}{\partial \omega} \\ \Sigma_{\mathrm{e}} = \Sigma_{33} - \Sigma_{11} = \dfrac{\sigma_0}{(1+n)}\left(\dfrac{\dot{\Xi}}{\dot{\xi}_0}\right)^n \left[(1+n)(\bar{U}^* + \tilde{U}^*) - \omega \dfrac{\partial(\bar{U}^* + \tilde{U}^*)}{\partial \omega}\right] \end{cases} \tag{65}$$

To obtain the generalized mean stress $\overline{\Sigma}_0$ and the mean strain rate $\dot{\overline{\xi}}_0$ of the matrix material, the concept of plastic work rate equality is introduced as

$$\begin{aligned} V_{\mathrm{m}} \overline{\Sigma_0} \dot{\overline{\xi}}_0 &= \int_{V_{\mathrm{cell}}} \left(\sigma'_{ij}\dot{\varepsilon}'_{ij} + \tau'^{(1)}_{ijk}\dot{\eta}'^{(1)}_{ijk} + \tau'^{(2)}_{ijk}\dot{\eta}'^{(2)}_{ijk} + \tau'^{(3)}_{ijk}\dot{\eta}'^{(3)}_{ijk}\right) \mathrm{d}V = (n+1)\int_{V_{\mathrm{cell}}} \varphi \, \mathrm{d}V = (n+1) V_{\mathrm{cell}} \Phi \\ &= V_{\mathrm{cell}} \Sigma_0 \dot{\xi}_0 \left(\frac{\dot{\Xi}}{\dot{\xi}_0}\right)^{n+1} (\bar{U}^* + \tilde{U}^*) \end{aligned} \tag{66}$$

Considering that the mean stress $\overline{\Sigma}_0$ and the mean strain rate $\dot{\overline{\xi}}_0$ of the matrix material should satisfy the plastic constitutive relation (11) and noting the Eq. (66), we obtain easily

$$\left(\frac{\overline{\Sigma}_0}{\Sigma_0}\right) = \left(\frac{\dot{\overline{\xi}}_0}{\dot{\xi}_0}\right)^n = \left[\frac{\Sigma_0 \dot{\xi}_0 V_{\mathrm{cell}} \left(\frac{\dot{\Xi}}{\dot{\xi}_0}\right)^{n+1} U^*}{V_m \dot{\xi}_0 \overline{\Sigma}_0}\right]^n = \left[\frac{\left(\frac{\dot{\Xi}}{\dot{\xi}_0}\right)^{n+1} U^*}{(1-f)\frac{\overline{\Sigma}_0}{\sigma_0}}\right]^n \tag{67a}$$

or

$$\overline{\Sigma}_0 = \left(\frac{\dot{\Xi}}{\dot{\xi}_0}\right)^n \left(\frac{U^*}{1-f}\right)^{n/(n+1)} \sigma_0 \tag{67b}$$

where $U^* = \bar{U}^* + \tilde{U}^*$.

Substituting (67b) into (65) yields

$$\begin{cases} \dfrac{\Sigma_{\mathrm{m}}}{\overline{\Sigma}_0} = \dfrac{\frac{2}{3}\frac{\partial U^*}{\partial \omega}}{(1+n)\left(\frac{U^*}{1-f}\right)^{n/(1+n)}} = \dfrac{2}{3\alpha}\dfrac{\partial U^*}{\partial \omega} \\ \dfrac{\Sigma_{\mathrm{e}}}{\overline{\Sigma}_0} = \dfrac{(1+n)U^* - \omega\frac{\partial U^*}{\partial \omega}}{(1+n)\left(\frac{U^*}{1-f}\right)^{n/(1+n)}} = \dfrac{1}{\alpha}\left[(1+n)U^* - \omega\dfrac{\partial U^*}{\partial \omega}\right] \end{cases} \tag{68}$$

where $\alpha = (1+n)\left(\frac{U^*}{1-f}\right)^{n/(1+n)}$.

Eliminating the additional parameter ω from the formula (68), we can obtain the size-dependent plastic potential of porous material as follows:

$$\varphi\left(\frac{\Sigma_{\mathrm{e}}}{\overline{\Sigma}_0}; \frac{\Sigma_{\mathrm{m}}}{\overline{\Sigma}_0}, \lambda, n, f\right) = 0 \tag{69}$$

Obviously, it is difficult to explicitly express the potential function (69) as classical Gurson model. For this reason, the Gaussian integration method must be adopted to calculate U^* in the expression (68) and thus obtain the yield loci $\varphi = 0$ or $\Sigma_{\mathrm{e}}/\overline{\Sigma}_0 \sim \Sigma_{\mathrm{m}}/\overline{\Sigma}_0$.

Generally speaking, the precision of displacement field (40) directly depends on the terms selected. Fig. 2 compares the influences of the number of terms taken on the curves $\Sigma_{\mathrm{e}}/\overline{\Sigma}_0 \sim \Sigma_{\mathrm{m}}/\overline{\Sigma}_0$. It can be seen easily that, for the displacement field (40), the solution corresponding to $K = M = 4$ is in good agreement with the solution corresponding to $K = M = 3$. This means that when $K = M = 3$, the solution is a very good approximation of the actual displacement field. If we carefully review the results of a two-terms solution (only including the terms $\bar{u}_i$ in (40) thus not a self-contained displacement field) by Huang et al. (2002), it is easy to see that although the two-terms solution is not self-contained, it is accurate enough. This powerfully proves that the assumption $a^* \ll 1$ made in the formula (58) is reasonable.

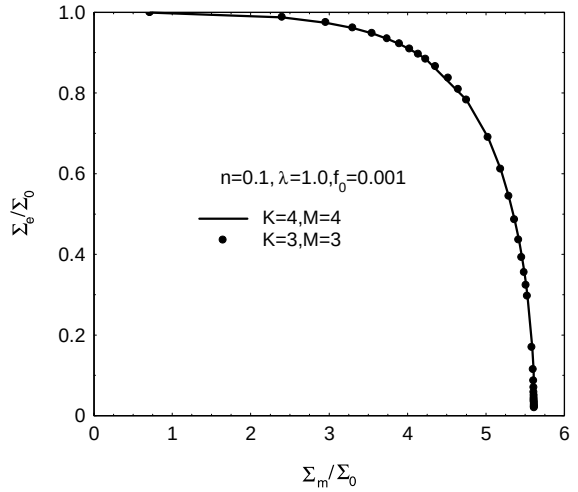

Fig. 2. The influences of the number of terms taken in (40) on the plasticity potential.

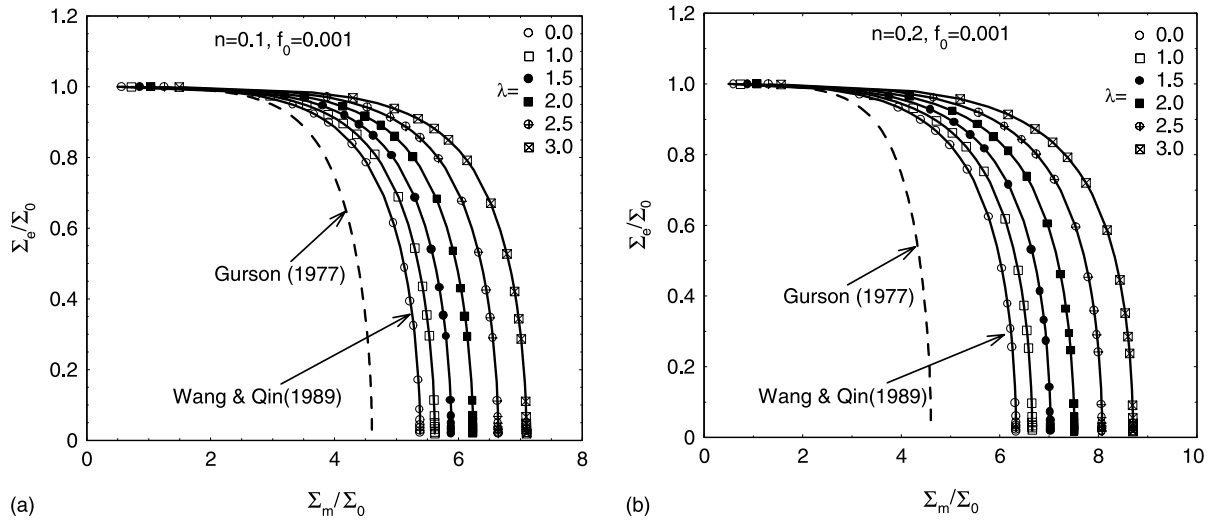

Fig. 3. The effects of void size on the plasticity potentials for: (a) $n = 0.1$ and (b) $n = 0.2$.

Fig. 3 shows the influences of the dimensionless characteristic length λ and the power-hardening exponent n on the macroscopic yield loci $\Sigma_e/\overline{\Sigma}_0 \sim \Sigma_m/\overline{\Sigma}_0$ of the porous materials. For the purposes of comparison, the results corresponding to the Gurson model are also displayed together. From Fig. 3, it can be easily seen that the dimensionless length factors λ have very obvious influences on the yield loci $\Sigma_e/\overline{\Sigma}_0 \sim \Sigma_m/\overline{\Sigma}_0$ especially when the triaxial stress levels $\Sigma_m/\overline{\Sigma}_0$ are higher. On the other hand, for the same triaxial stress level, with the dimensionless length factors $\lambda = l/a$ increasing, the corresponding yield stress $\Sigma_e/\overline{\Sigma}_0$ becomes higher. This means that, for a fixed void volume fraction f_0, the porous materials with smaller voids possess higher yield stress, especially when the void size a is comparable with the characteristic length l.

As everyone knows, the void growth can be described by $\omega^* = \frac{\omega}{f} = \frac{\dot{V}_v}{\dot{E}_e V_v}$ (here V_v denotes the volume of void). Fig. 4 shows the influences of the dimensionless length factor $\lambda = l/a$ on the growth of the void. The

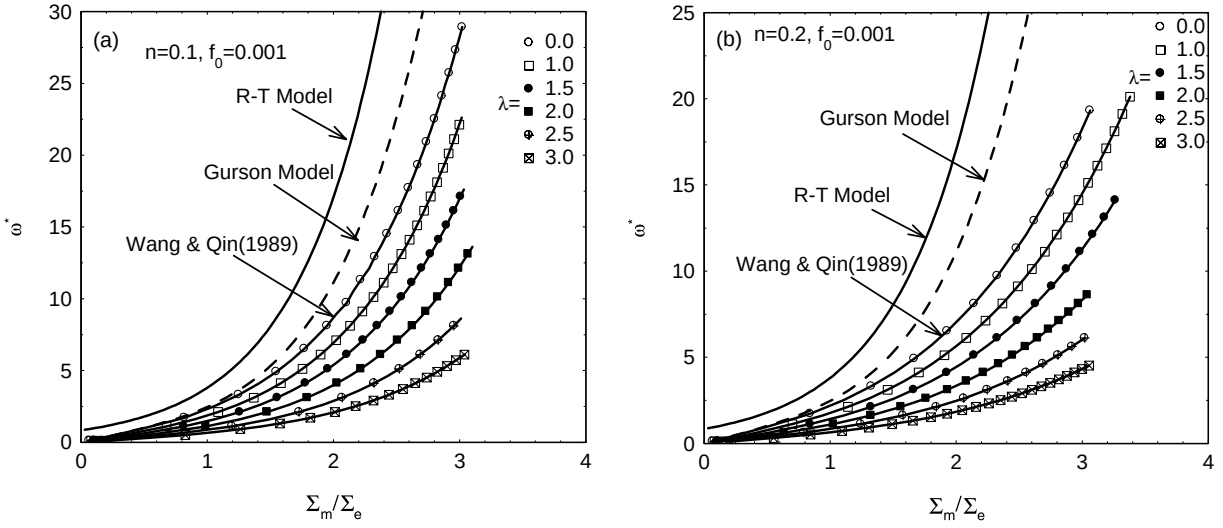

Fig. 4. The effects of void size on the void growth for: (a) $n = 0.1$ and (b) $n = 0.2$.

results associated with the Gurson model and R–T model are also presented together. For a fixed initial void volume fraction f_0, it is not difficult to see a substantial reduction of the void growth rate with $\lambda = l/a$ increasing. This is to say that the void growth is size dependent, and the growth rate of smaller voids is slower than that of larger voids. The classical plastic damage theories cannot predict the size dependence of the void growth since they do not involve any intrinsic material length scale. Added to this, the void growth rates predicted by the classical size-independent damage model are higher than that given by the present scale-dependent damage model.

4. Summary

In the present paper, we have been actively engaged in the development of a size-dependent plastic potential for porous materials. Following the same line of thought as the Gurson model, the macroscopic responses of a representative spherical cell under remote axisymmetric triaxial tension have been carefully investigated. To capture the size effects of local plastic deformation within the matrix, the SG constitutive theory including the rotation and the stretch gradients by Fleck and Hutchinson (1997) has been adopted. By means of the principle of minimum plasticity potential, the displacement field satisfying the equilibrium equations, displacement compatibility equations and displacement boundary conditions has been computationally determined by the Lagrange multiplies method. Based on this, we have obtained a size-dependent plastic potential for a porous material and examined the size effect on the void growth. The results show clearly that the void size has very important influences on the growth of spherical void, especially when the radius a of the microvoid is comparable with the intrinsic characteristic length l of matrix. In summary, the originality of this work consists of generalizing the classical Gurson model to include the size effects on the void evolution and the flow stress of porous materials.

It is worth pointing out that the present model is based on the assumption that the macroscopic higher order strain or stress on the size scale of the representative cell can be ignored. This is true when the initial void volume fraction f_0 is low and the size of the cell is large. Therefore, the present model is especially applicable to the case in which the size of void is small and the microvoids in material are very dilute. Fortunately, with plastic deformation increasing, the microvoids with smaller size will grow gradually. Once the radius of microvoid is much larger than the intrinsic characteristic length l of the matrix material, the present model will automatically reduce to the size-independent Gurson model improved by Wang and Qin (1989). Therefore, no matter whether the size of voids is small or large, the present model can provide a better description of the growing process of microvoids.

Acknowledgements

The National Natural Science Foundation of China under Grant No. A10102006 supported the present research and helpful comments of anonymous reviews are also gratefully acknowledged.

References

Acharya, A., Bassani, J.L., 2000. Lattice incompatibility and a gradient theory of crystal plasticity. J. Mech. Phys. Solids 48, 1565–1595.

Acharya, A., Beaudoi, A.J., 2000. Grain-size effect in viscoplastic polycrystals at moderate strains. J. Mech. Phys. Solids 48, 2213–2230.

Bažant, Z.P., Lin, F.B., 1988. Non-local yield limit degradation. Int. J. Numer. Mech. Engng. 26, 1805–1823.

Begley, M.R., Hutchinson, J.W., 1998. The mechanics of size-dependent indentation. J. Mech. Phys. Solids 46, 2049–2068.
Bittencourt, E., Needleman, A., Gurtin, M.E., Van der Giessen, E., 2003. A comparison of nonlocal continuum and discrete dislocation plasticity predictions. J. Mech. Phys. Solids 51, 281–310.
Cleveringa, H.H.M., Ver der Giessen, E., Needleman, A., 1997. Comparison of discrete dislocation and continuum plasticity predictions for a composite material. Acta Mater. 45, 3163–3179.
Cleveringa, H.H.M., Ver der Giessen, E., Needleman, A., 1998. Discrete dislocation simulations and size-dependent hardening in single slip. J. Phys. 4, 83–92.
Cleveringa, H.H.M., Ver der Giessen, E., Needleman, A., 1999a. A discrete dislocation analysis of residual stress in a composite material. Philos. Mag. A 79, 863–920.
Cleveringa, H.H.M., Ver der Giessen, E., Needleman, A., 1999b. A discrete dislocation analysis of bending. Int. J. Plastic. 15, 837–868.
De Guzman, M.S., Neubauer, G., Finn, P., Nix, W.D., 1993. The role of indentation depth on the measured hardness of materials. Mater. Res. Symp. Proc. 308, 613–618.
Duva, J.M., Hutchinson, J.W., 1984. Constitutive potentials for dilutely voided nonlinear materials. Mech. Mater. 3, 41–54.
Faleskog, J., Gao, X., Shih, C.F., 1998. Cell model for nonlinear fracture analysis—I. Micromechanics calibration. Int. J. Fract. 89, 355–373.
Fleck, N.A., Hutchinson, J.W., 1993. A phenomenological theory for strain gradient effects in plasticity. J. Mech. Phys. Solids 41, 1825–1857.
Fleck, N.A., Muller, G.M., Ashby, M.F., Hutchinson, J.W., 1994. Strain gradient plasticity: theory and experiment. Acta Mater. 42, 475–487.
Fleck, N.A., Hutchinson, J.W., 1997. Strain gradient plasticity. In: Hutchinson, J.W., Wu, T.Y. (Eds.), Advances in Applied Mechanics, vol. 33. Academic Press, New York, pp. 295–361.
Fleck, N.A., Hutchinson, J.W., 2001. A reformulation of strain gradient plasticity. J. Mech. Phys. Solids 49, 2245–2271.
Gao, H., Huang, Y., Nix, W.D., Hutchinson, J.W., 1999. Mechanism-based strain gradient plasticity—I theory. J. Mech. Phys. Solids 47, 1239–1263.
Gao, H., Huang, Y., 2001. Taylor-based nonlocal theory of plasticity. Int. J. Solids Struct. 38, 2615–2637.
Gao, H., Huang, Y., 2003. Geometrically necessary dislocation and size-dependent plasticity. Scr. Mater. 48, 113–118.
Gao, X., Faleskog, J., Shih, C.F., 1998a. Cell model for nonlinear fracture analysis—II. Fracture-process calibration and verification. Int. J. Fract. 89, 375–398.
Gao, X., Faleskog, J., Shih, C.F., 1998b. Ductile tearing in part-through crack, experiments and cell model prediction. Engng. Fract. Mech. 59, 761–777.
Gologanu, M., Leblond, J.B., Perrin, G., 1995. A micromechanically based Gurson-tpye model for ductile porous materials including strain gradient effects. In: Krishnaswami, S., McMeeking, R.M., Trasorras, J.R.L. (Eds.), Net Shape Processing of Power Materials, ASME AMD 216,47. American Society of Mechanical Engineering, New York.
Gurson, A.L., 1977. Continuum theory of ductile rupture by void nucleation and growth: Part I—yield criteria and flow rules for porous ductile media. J. Engng. Mater. Technol. 99, 2–15.
Huang, M.S., Li, Z.H., Wang, C., Chen, C.Y., 2002. The influences of microscopic size effect of matrix on plastic potential and void growth of porous materials. Acta Mech. Solid. Sin. 15, 283–302.
Huang, Y., Gao, H., Nix, W.D., Hutchinson, J.W., 2000a. Mechanism-based strain gradient plasticity–II. Anal. J. Mech. Phys. Solids 48, 99–128.
Huang, Y., Xue, Z., Gao, H., Nix, W.D., Xia, Z.C., 2000b. A study of micro-indentation hardness tests by mechanism-based strain gradient plasticity. J. Mater. Res. 15, 1786–1796.
Huang, Y., 1991. Accurate dilatation rates for spherical void in triaxial stress fields. J. Appl. Mech. 58, 1084–1086.
Koplik, J., Needleman, A., 1988. Void growth and coalescence in porous plastic solids. Int. J. Solids Struct. 24, 835–853.
Leblond, J.B., Perrin, G., Dexaux, J., 1994. Bifurcation effects in ductile metals with damage delocalization. J. Appl. Mech. 61, 236.
Leblond, J.B., Perrin, G., Dexaux, J., 1995. Improved Gurson-type model for hardenable ductile metal. Eur. J. Mech. A/Solids 14, 499–527.
Lee, J.B., Mear, M.E., 1992. Axisymmetric deformation of power-law solids containing a dilute concentration of aligned spheroidal voids. J. Mech. Phys. Solids 40, 1805–1836.
Li, Z.H., Wang, C., Chen, C.Y., 2002. The influence of the yield stress gradient on the growth and coalescence of spherical voids in the materials. Int. J. Solids Struct. 39, 601–616.
Li, Z.H., Wang, C., Chen, C.Y., 2003. The evolution of voids in the plasticity strain hardening gradient materials. Int. J. Plastic. 19, 213–234.
Lloyd, D.J., 1994. Particle reinforced aluminum and Magnesium matrix composites. Int. Mater. Rev. 39, 1–23.
Ma, Q., Clark, D.R., 1995. Size-dependent hardness in silver single crystals. J. Mater. Res. 10, 853–863.
McClintock, F.A., 1968. A criterion of ductile fracture by growth of holes. ASME, J. Appl. Mech. 35, 363.

Mcelhaney, K.W., Vlassak, J.J., Nix, W.D., 1998. Determination of indenter tips geometry and indentation contact area for depth-sensing indentation experiments. J. Mater. Res. 13, 1300–1306.
Nan, C.W., Clarke, D.R., 1996. The influence of particle size and particle fracture on the elastic/plastic deformation of metal matrix composites. Acta Mater. 44, 3801–3811.
Nix, W.D., 1989. Mechanical Properties of Metal. Wiley, New York.
Nix, W.D., 1997. Elastic and plastic properties of thin films on substrates: nano-indentation techniques. Mat. Sci. Engr. A 234–236, 37–44.
Nix, W.D., Gao, H., 1998. Indentation size effects in crystalline materials: A law for strain gradient plasticity. J. Mech. Phys. Solids 46, 411–425.
Pardoen, T., Hutchinson, J.W., 2000. An extended model for void growth and coalescence. J. Mech. Phys. Solids 48, 2467–2512.
Poole, W.J., Ashby, M.F., Fleck, N.A., 1996. Microhardness of annealed and work-hardened copper polycrysrals. Scr. Metall. Mater. 34, 559–564.
Pijaudier-Cabot, G., Bažant, Z.P., 1987. Nonlocal damage theory. ASCE J. Eng. Mech. 10, 1512–1533.
Rice, J.R., Tracey, D.M., 1969. On the ductile enlargement of voids in triaxial stress fields. J. Mech. Phys. Solids 17, 201–207.
Ruggieri, C., Panontin, T.L., Dodds, R.H., 1996. Numerical modeling of ductile crack growth in 3-D using computational cell elements. Int. J. Fract. 82, 67–96.
Shu, J.Y., 1998. Scale-dependent deformation of porous single crystals. Int. J. Plastic. 14, 1085–1107.
Smyshlyaev, V.P., Fleck, N.A., 1996. The role of strain gradients in the grain size effect for polycrystals. J. Mech. Phys. Solids 44, 465–496.
Stelmashenko, N.A., Walls, M.G., Brown, L.M., Molman, Y.V., 1993. Microindentation on W and Mo oriented single crystals: an STM study. Acta Metall. Mater. 41, 2855–2865.
Stolken, J.S., Evans, A.G., 1998. A Microbend test method for measuring the plasticity length scale. Acta Mater. 46, 5109–5115.
Sun, D.Z., Hönig, A., 1994. Significance of the characteristic length for micromechanical modeling of ductile fracture. In: Computer Aided Assessment and Control of Localized Damage—Proceedings of the International Conference, 21–23 June 1994.
Suresh, S., Nieh, T.G., Choi, B.W., 1999. Nano-indentation of copper thin films on silicon substrates. Scr. Mater. 41, 951–957.
Tvergaard, V., 1981. Influence of voids on shear band instabilities under plane strain conditions. Int. J. Fract. 17, 389–407.
Tvergaard, V., 1982. On localization in ductile materials containing voids. Int. J. Fract. 18, 237–252.
Tvergaard, V., Needleman, A., 1984. Analysis of the cup–cone fracture in a round bar. Acta Metall. 32, 157–169.
Tvergaard, V., Needleman, A., 1997. Nonlocal effects on localization in a void sheet. Int. J. Solids Struct. 34, 2221.
Wang, T.C., Qin, J.L., 1989. The constitutive potential and growth rate of non-linear materials containing voids. Acta Mech. Solid. Sin. 10, 127–141 (in Chinese).
Xia, L., Shih, C.F., 1995a. Ductile crack growth—I. A numerical study using computational cells with microstructurally based length scales. J. Mech. Phys. Solids 43, 233–259.
Xia, L., Shih, C.F., 1995b. Ductile crack growth—II. Void nucleation and geometry effects on macroscopic fracture behavior. J. Mech. Phys. Solids 43, 1953–1981.
Xia, L., Shih, C.F., 1996. Ductile crack growth — III. Transition to cleavage fracture incorporating statistics. J. Mech. Phys. Solids 44, 603–639.
Yamamoto, H., 1978. Conditions for shear localization in the ductile fracture of void-containing materials. Int. J. Fract. 14, 347–365.
Zhu, H.T., Zbib, H.M., 1995. Flow strength and size effect of an Al–Si–Mg composite model system under multiaxial loading. Scr. Metall. Mater. 32, 1895–1902.
Zhu, H.T., Zbib, H.M., Aifantis, E.C., 1997. Strain gradients and continuum modeling of size effect in metal matrix composites. Acta Mech. 121, 161–176.